Design and modeling of an all-optical frequency modulated MEMS strain sensor using nanoscale Bragg gratings

Reck-Nielsen, Kasper; Almind, Ninia Sejersen; Mar, Mikkel Dysseholm; Hübner, Jörg; Hansen, Ole; Thomsen, Erik Vilain

Published in:
I E E E Sensors. Proceedings

Link to article, DOI:
10.1109/ICSENS.2009.5398237

Publication date:
2009

Document Version
Publisher's PDF, also known as Version of record

Design and Modeling of an All-Optical Frequency Modulated MEMS Strain Sensor using Nanoscale Bragg Gratings

Kasper Reck, Ninia S. Almind, Mikkel Mar, Jörg Hübner, Ole Hansen and Erik V. Thomsen
Department of Micro and Nanotechnology
Technical University of Denmark (DTU)
2800, Kgs. Lyngby
Email: kasper.reck@nanotech.dtu.dk

***Abstract*— We present modeling and design of an all-optical MEMS Bragg grating (half-pitch of 125 nm) strain sensor for single-fiber distributed sensing. Low optical loss and the use of frequency modulation rather than amplitude modulation, makes this sensor better suited for distributed systems than comparable designs, e.g. Fabry-Perot and Mach-Zender. Also, multiplexing of several sensors with different period gratings, allow sensors to be connected to a single fiber, thereby minimizing cabling and simplifying readout. We show through analytical analysis and finite element modeling (FEM) that large mechanical amplification can be obtained if using an angled double beam micrometer scale MEMS structure, compared to conventional fiber Bragg grating sensors. An optimized design and fabrication process is presented.**

I. Introduction

Optical sensors based on MEMS technology has within the past two decades received increased attention as they present an alternative to conventional electrical sensing. The main advantages of optical sensors are typically high sensitivity, immunity to electromagnetic interference, safe operation in environments with explosion risk and low loss which makes them suitable for remote sensing. Several sensing concepts have been explored in literature, including strain sensors, chemical sensors, inertial sensors and pressure sensors [1]. However, the high accuracy is often achieved using amplitude modulation of the input signal, hence only one sensor can be attached to the transmission line. Also, the use of diffraction gratings in many of these sensors calls for the use of electrical photodiodes integrated on the chip, which limits the use of the sensors to areas where electrical sensors already dominate. Frequency modulation based sensing has been extensively used in fiber Bragg grating (FBG) sensors, with applications mainly within structural health monitoring. While FBGs can easily be used for distributed and remote sensing, the gratings are relatively large compared to what can be obtained by MEMS sensors due to material properties, resulting in lower sensitivity and larger physical size. In this work we present a design and optimization of an all-optical MEMS Bragg grating (MBG) sensor, with high sensitivity, suitable for distributed and remote sensing. The central sensing element is a doubly-clamped double beam with an optical waveguide with integrated Bragg grating as shown in Figure 1. When a broadband light source is connected to the waveguide, the wavelength of the Bragg reflected light is given by $\lambda_B = 2n_{eff}\Lambda$, where Λ is the period of the Bragg grating. By applying a force at the boss, a compressive strain is created in the Bragg grating which changes the period and therefore also the reflected wavelength. Neglecting photoelastic effects one has $\frac{\Delta\lambda_B}{\lambda_B} = \varepsilon_l$, where ε_l is the longitudinal strain.

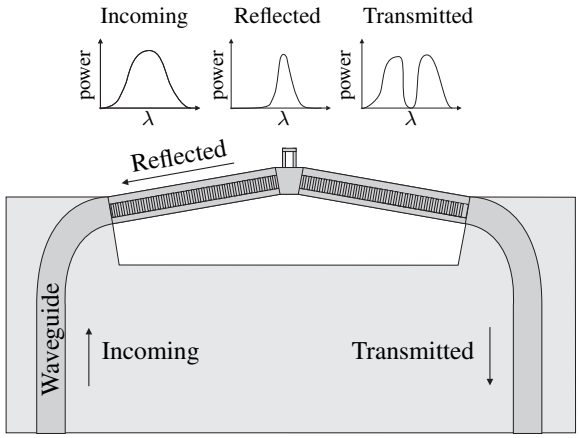

Fig. 1. The sensor consists of a waveguide with integrated Bragg grating. Deformation of the Bragg grating causes a change in the wavelength of the reflected signal. Several sensors with different Bragg grating periods can be connected to a single fiber with both the transmission and data analysis at only one end.

II. Analytical Model

Thus in order to maximize the sensitivity of the sensor, i.e. the wavelength shift, the strain along the waveguide (perpendicular to the grating) should be as large as possible, while the bending should be small so to avoid distortion of the signal. Considering the general double beam in Figure 2, two limiting cases exists: A simple straight doubly-clamped beam, i.e. $\theta = 0°$, in which only pure bending will occur (considering small deflections) and the sensitivity would be zero, and a beam with $\theta = 90°$, in which the strain will be purely longitudinal, but small due to the high stiffness of

$$w = \frac{w_{end}\left(-2 + e^{kL} + e^{-kL} - kxe^{kL} + kxe^{-kL} + e^{-kx} - e^{-kx}e^{kL} + e^{kx} - e^{kx}e^{-kL}\right)}{-2 + 2\,e^{kL} + 2\,e^{-kL} - kLe^{kL} + kLe^{-kL} - 2\,e^{-kL}e^{kL}}. \tag{8}$$

$$w = w_{end}\frac{1 - \cos(Lk) - i\sin(Lk) + ikx(\cos(Lk) + i\sin(Lk) + 1) - (\cos(kx) + i\sin(kx)) + \frac{\cos(kL)+i\sin(kL)}{\cos(kx)+i\sin(kx)}}{-2(\cos(kL) + i\sin(kL)) + iLk(\cos(kL) + i\sin(kL)) + 2 + iLk} \tag{14}$$

the structure. Thus, as the angle is decreased from 90° to 0° the structure will be less stiff and the longitudinal strain will increase until a certain angle of maximum longitudinal strain where bending will start to dominate. The deflection of this double beam can be described by the following Euler beam equation

$$EI\frac{\mathrm{d}^4w}{\mathrm{d}x^4} - N\frac{\mathrm{d}^2w}{\mathrm{d}x^2} = q, \tag{1}$$

where E is Young's modulus, I the moment of inertia, N is the longitudinal force, w is the beam deflection, x is the position along the beam and q is the load. Assuming the center boss is non-deformable and exploiting the symmetry of the structure, the problem is simplified to a clamped-guided beam, i.e. the position of the guided end is given by the position of the center boss, which is restricted to vertical movement due to symmetry. This leads to the following relation between longitudinal deformation, u, and the end deflection, w_{end},

$$u = w_{end}\tan\theta. \tag{2}$$

Since

$$u = L\varepsilon = \frac{LN}{EWH}, \tag{3}$$

where L, W and H are the length, width and height of the beam, one has

$$w_{end} = \frac{LN}{EWH\tan\theta}. \tag{4}$$

A simpler solution of Equation 1 can be obtained by calculating the force required for a specific deflection instead of the required deflection due to a specific force. This is done by setting $q = 0$ and setting $w(L) = w_{end}$. As the beam is fixed at the left end and symmetry and continuity requires the first derivative at the right to be zero, the equation system to be solved is

$$\frac{\mathrm{d}^4w}{\mathrm{d}x^4} - k^2\frac{\mathrm{d}^2w}{\mathrm{d}x^2} = 0 \tag{5}$$

$$w(0) = 0 \qquad w(L) = w_{end} \tag{6}$$

$$\left.\frac{\mathrm{d}w}{\mathrm{d}x}\right|_{x=0} = 0 \qquad \left.\frac{\mathrm{d}w}{\mathrm{d}x}\right|_{x=L} = 0. \tag{7}$$

where $k^2 = N/(EI)$. The solution is given in Equation 8. It is noted that w is a function of N, which is still unknown. For a static deflection the vertical forces on the center boss are in balance as shown in Figure 3, i.e.

$$F + (V_r - V_l)\cos(\theta) + (N_r + N_l)\sin(\theta) = 0, \tag{9}$$

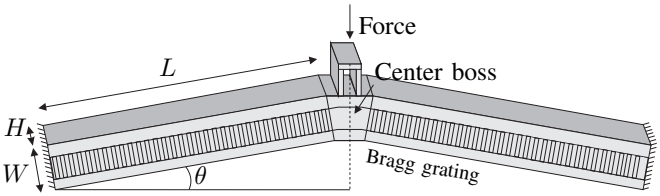

Fig. 2. The longitudinal strain is enhanced by mechanical amplification in this double beam structure. A force is applied at the center boss, causing compression of the Bragg grating and thereby a shift in the wavelength of the reflected signal.

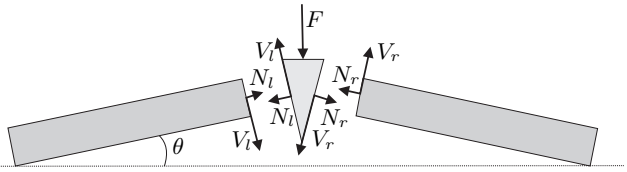

Fig. 3. The shear forces, V, and the normal forces, N, balance the applied force, F.

where V is a shear force (left and right). By symmetry $V_l = -V_r$ and $N_l = N_r$, hence

$$F - 2V_l\cos(\theta) + 2N_l\sin(\theta) = 0. \tag{10}$$

The shear force and the bending moment, M, are related by

$$\frac{\mathrm{d}M}{\mathrm{d}x} = V, \tag{11}$$

and for small deflections

$$M \approx -EI\frac{\mathrm{d}^2w}{\mathrm{d}x^2}, \tag{12}$$

hence the tension can be found as

$$N_l = \frac{\frac{F}{2} + EI\frac{\mathrm{d}^3w}{\mathrm{d}x^3}\cos(\theta)}{\sin(\theta)}, \tag{13}$$

where the sign has been switched so $N_l > 0$ represents a tensile force in the beam. Using Equation 13 and 8, one can solve for w and N, however, the exponential terms makes this rather cumbersome. For simplicity a compressive strain is assumed, hence k is complex and Equation 8 can be rewritten in terms of trigonometric functions as in Equation 14. In order to obtain a simple analytical expression that can be easily analyzed, a Laurent expansion to the sixth order with respect to k is used, yielding

$$w = \frac{Nx^2(-2x + 3L)}{L^2EWH\tan(\theta)} \tag{15}$$

and

$$N = \frac{FL^2WH\tan(\theta) - 24IN\cos(\theta)}{2L^2WH\tan(\theta)\sin(\theta)} \tag{16}$$

where

$$I = \frac{WH^3}{12}. \tag{17}$$

Solving Equations 15 and 16 with respect to w and N results in

$$w = \frac{Fx^2(2x-3L)\cos(\theta)}{2E(-H^2\cos(\theta)^2 - L^2 + L^2\cos(\theta)^2)WH} \tag{18}$$

and

$$N = \frac{FL^2\tan(\theta)}{2L^2\tan(\theta)\sin(\theta) + 2H^2\cos(\theta)}. \tag{19}$$

From Equation 3 the strain in the beam is

$$\varepsilon = \frac{FL^2\tan(\theta)}{(2L^2\tan(\theta)\sin(\theta) + 2H^2\cos(\theta))EWH}. \tag{20}$$

The validity of this result is verified by comparison to results obtained by FEM in the commercial software COMSOL. In Figure 4(a) the longitudinal strain as function of θ has been plotted. Assuming the beam is made in a polymer (e.g. SU-8) with $E = 4$ GPa, and $W = H = 15$ μm, the angle of maximum strain is seen in Figure 4(b) to shift towards smaller angles as the length to width ratio of the beam is increased. The angle of maximum strain as function of length can be found by differentiating Equation 3 with respect to θ, i.e.

$$\theta_{max} = \tan^{-1}\left(\frac{H}{\sqrt{-2H^2 + L^2}}\right) \pm n\pi, \tag{21}$$

where n is an integer, which considering the angles of interest is set to zero. Assuming $L > H$, one has

$$\theta_{max} \approx \tan^{-1}\left(\frac{H}{L}\right). \tag{22}$$

Using this approximation, Equation 20 can be written

$$\varepsilon(\theta_{max}) \approx \frac{FL^2\frac{W}{L}}{(2L^2\frac{W}{L}\frac{W}{L\sqrt{1+\frac{W^2}{L^2}}} + 2H^2\frac{1}{\sqrt{1+\frac{W^2}{L^2}}})EWH}, \tag{23}$$

which for large aspect ratios reduces to

$$\varepsilon(\theta_{max}) \approx \frac{FL}{2E(W^3 + H^3)}. \tag{24}$$

At an aspect ratio of 10, the error of Equation 24 compared to Equation 20 is approximately 20% while at an aspect ratio of 20 (or above) it is less than 1%.

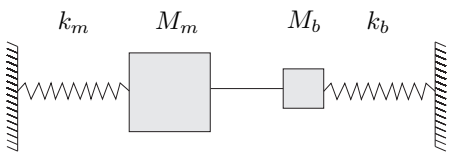

Fig. 5. The membrane with mass M_m is directly connected to the beam with mass M_b. The two springs with spring constants k_m and k_b are due to the membrane fixture and the beam itself, respectively.

A. Frequency Response

Often, the Rayleigh-Ritz method is applied in order to calculate the frequency response. However, due to the use of the Laurant expansion that is not possible here and a simpler spring-mass model will be applied instead. We will consider a system in which the sensor is attached to the backside of a 1" microphone membrane. The membrane has the mass M_m and is kept in place through a spring with a spring constant k_m. Likewise, the beam has the mass M_b and has a spring constant k_b. The beam is attached directly to the membrane, as illustrated in Figure 5, and the beam and membrane are therefore considered as one object with the mass $M_{tot} = M_m + M_b$. From Newtons second law one finds

$$M_{tot}\frac{\mathrm{d}^2x}{\mathrm{d}t^2} = -k_bx - k_mx, \tag{25}$$

The resonance frequency then is

$$f = \frac{1}{2\pi}\sqrt{\frac{k_b + k_m}{M_{tot}}}. \tag{26}$$

For long beams, θ will be small according to Equation 22 and we can calculate k_b from Equation 18 only, hence

$$k_b \approx \frac{2EWH(L^2\sin(\theta)^2 + H^2\cos(\theta)^2)}{L^3\cos(\theta)}. \tag{27}$$

The spring constant for a circular clamped plate of radius a and thickness h is

$$k_m = \frac{16}{3}\frac{E}{(1-\nu^2)}\frac{\pi h^3}{a^2}, \tag{28}$$

where ν is the Poisson ratio. Inserting in Equation 26 yields

$$f = \frac{1}{2\pi}\sqrt{\frac{\frac{2EWH(L^2\sin(\theta)^2+H^2\cos(\theta)^2)}{L^3\cos(\theta)} + \frac{16}{3}\frac{E}{(1-\nu^2)}\frac{\pi h^3}{a^2}}{M_{tot}}}. \tag{29}$$

A typical 1" radius and 3 μm thick nickel membrane weighs 5 mg. Assuming $L = 150$ μm, $H = W = 20$ μm, $\theta = 3.8°$ and $E = 26$ GPa for the beam (assuming it is made of one part SiO_2 and two parts polymer) the resonance frequency is $f = 4.89$ kHz. For a 75 μm long beam the resonance frequency is $f = 14.9$ kHz. At a sound pressure level of $P = 0.005$ Pa (equal to 48 dB) the longitudinal beam strain is approximately 10^{-6} in the 150 μm beam and likewise at $P = 0.01$ (54 dB) for the 75 μm beam, assuming the force on the membrane is carried on to the beam. By adjusting the dimensions and materials of the beam, the resonance frequency and sensitivity can be tuned for the application at hand. Using

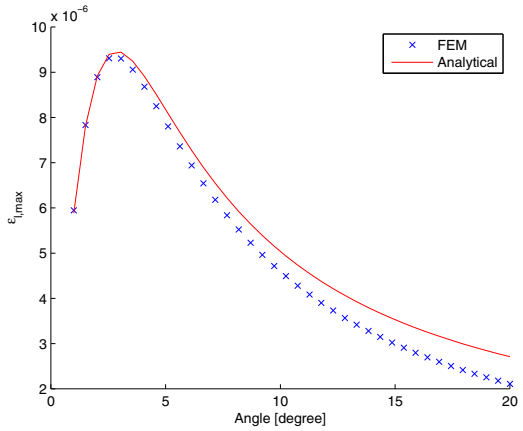

(a) This comparison of the strain calculated from analytical expressions and by FEM shows only minor deviations which can be contributed to the inclusion of Poisson contraction and deformable center boss in the FEM model.

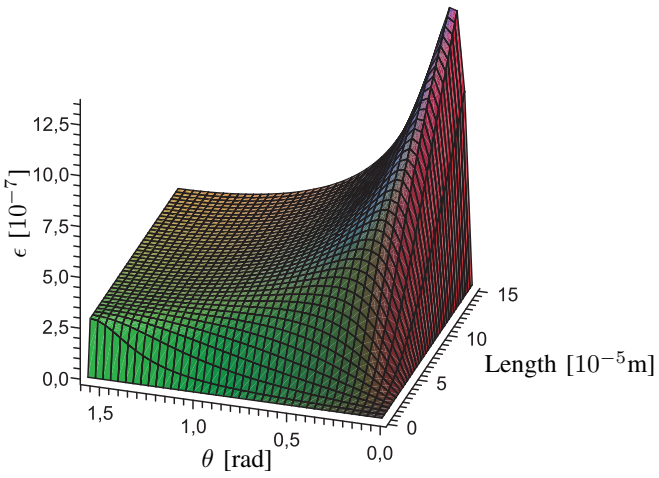

(b) The longitudinal strain calculated using Equation 20. As the length of the beam is increased relative to the width and height, the angle of maximum strain decreases.

Fig. 4.

Material	$\sqrt{\frac{E}{M}}$ [m/s]	L [μm]	f [kHz]	SPL$_{min}$ [dB]
Nickel	4904	75	14.9	54
Nickel	4904	150	4.9	48
Si_3N_4	7806	75	23	53
Si_3N_4	7806	150	8.3	47
Kevlar 49	9440	75	34.2	46
Kevlar 49	9440	150	12.3	40

TABLE I

THE RESONANCE FREQUENCIES AND MINIMUM DETECTABLE SOUND PRESSURE LEVEL (FOR $1\mu\varepsilon$) FOR DIFFERENT MEMBRANE MATERIALS.

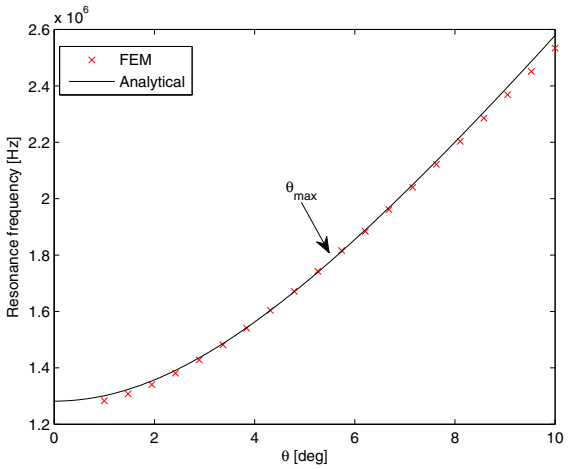

Fig. 6. The resonance frequency in a 150 μm long silicon beam with a cross-section of 15×15 μm^2 calculated by FEM and Equation 26 with $k_m = 0$. The angle of maximum strain is indicated by the arrow.

another material for the membrane could potentially yield better performance, here light weight and stiff materials would increase the resonance frequency. If the membrane is made of silicon nitride ($E = 194$ GPa and $\rho = 3184$), which has a stiffness comparable to nickel, but is 2.8 times lighter, the resonance frequencies would be 8.3 KHz and 23 KHz for the 150 μm and 75 μm beam, respectively, with a small increase in sensitivity. Even better is a material like Kevlar 49 ($E = 131$ GPa and $\rho = 1470$). Here the resonance frequencies would be 12.3 KHz and 34.2 KHz and the pressure at 10^{-6} strain would be 0.002 Pa and 0.004 Pa (or 40 dB and 46 dB), respectively. The resonance frequencies and minimum SPL, assuming a detection limit of $1\mu\varepsilon$, are listed in Table I for different membrane materials. The resonance frequencies are also calculated numerically using FEM. The resonance frequency as function of θ is plotted in Figure 6 for a silicon beam with $L = 150$ μm and $W = H = 15$ μm. The analytical expression is seen to agree well with the FEM results. At θ_{max} the resonance frequency of the beam is found to 1.81 MHz. The strain as function of sound pressure level is shown in Figure 7 for a SiO_2/polymer beam, with reasonable agreement between the analytical and the FEM results. At a sound pressure level of approximately 120 dB, the FEM results starts to deviate from the analytical results due to buckling. Based on these results a reasonable maximum sound pressure level for the sensor would be up to 110 dB.

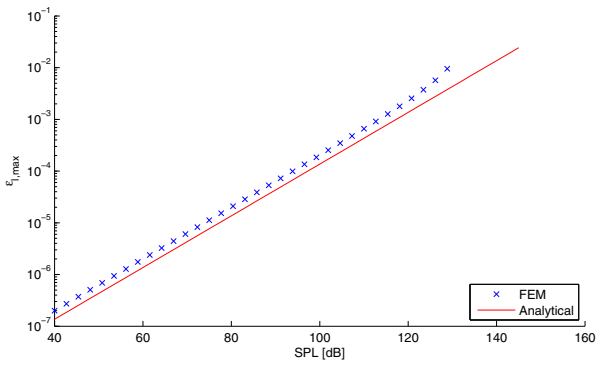

Fig. 7. At approximately 120 dB, buckling sets in and the FEM results starts to deviate from the analytical.

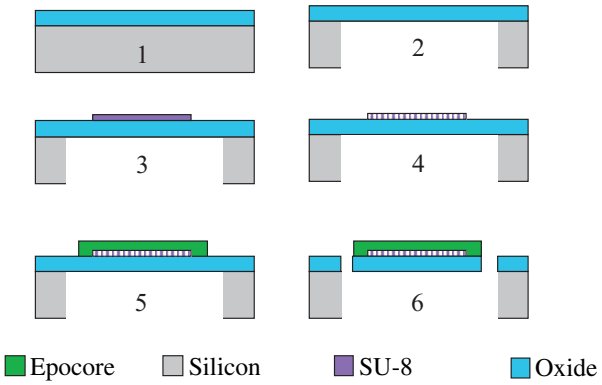

Fig. 8. PECVD oxide is deposited on a silicon wafer and a membrane is created using ASE. The waveguide cores are made in SU8 using UVL and gratings are made using combined UVL/NIL. Epocore is spin-coated and acts as upper cladding. The beam is released using RIE.

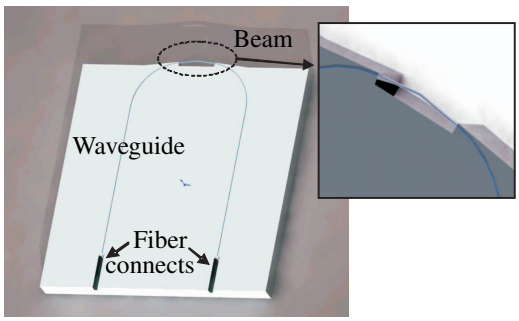

Fig. 9. The final device with optical fiber connections at the bottom of the chip and the beam at the top.

III. Process Flow

We now consider a process flow for fabrication of a SiO_2/SU-8/Epocore waveguide for use at a wavelength of approximately 800 nm. In order to obtain single mode propagation, the waveguide core should be approximately 3 μm wide while the period of the Bragg grating should be $\Lambda = 250$ nm. Thus, the waveguide itself can be made using standard UV-lithography (UVL), while the Bragg grating can be made by e.g. e-beam lithography (EBL). If mass production is of concern, nano imprint lithography could be a better choice. The SiO_2/polymer combination is chosen due to its relatively low stiffness and high mechanical stability. An all-polymer beam would have higher sensitivity, but could also easily fail due to mechanical instability.

The process flow is illustrated in Figure 8. Approximately 7 μm of PECVD oxide is deposited on a silicon wafer and fiber connect grooves are made on the front side using Advanced Oxide Etch (AOE) and Advanced Silicon Etching (ASE), while ASE is used on the backside for creating a sacrificial membrane beneath the beam. The oxide will serve as the lower cladding layer of the waveguide. The core and Bragg grating can be made either in a single combined UV and nano imprint lithography step or by sequential UV and EBL. Epocore is then spin-coated on the wafer and patterned, and will act as the upper cladding. Reactive Ion Etching (RIE) on the front side is used to release the beam from the membrane. By applying Epocore before and after the SU-8 core layer, an all-polymer beam can be created by RIE from the back side instead for the front side. The final device measures 5×5 mm^2 and is illustrated in Figure 9.

IV. Conclusion

We have presented an all-optical sensor concept for distributed and remote strain sensing, based on wavelength shift due to deformation of a MEMS fabricated waveguide with integrated Bragg grating. The sensor is considered a low cost, small size and high sensitivity alternative to FBGs, and will in many places be able to replace electrical sensors due to its high sensitivity. The Euler beam equation has been used for obtaining an analytical model describing the sensitivity of the model. The model has been verified using FEM, and it was shown that if connected to a 1" microphone membrane, sound pressure levels down to the 40-50 dB range can be measured assuming a strain resolution of 1 $\mu\varepsilon$. A spring mass model of the microphone system showed that resonance frequencies between 5 and 34 kHz are obtainable, depending on the membrane material. Finally a process flow for fabrication of the suggested sensor design was presented. By using NIL or similar sub-micron parallel fabrication methods for fabrication of the Bragg gratings, the sensor could easily be produced in large quantities.

Acknowledgment

We would like to acknowledge support from the Danish National Advanced Technology Foundation.

References

[1] M. E. Motamedi, *MOEMS: Micro-Opto-Electro-Mechanical Systems* SPIE Press, 2005.